AIAA JOURNAL
Vol. 36, No. 3, March 1998

Detrimental Effects of Almost Immeasurably Small Freestream Nonuniformities Generated by Wind-Tunnel Screens

Jonathan H. Watmuff*
MCAT Inc., Moffett Field, California 94035

Measurements are presented that were obtained during the course of a series of flow quality improvements to a small stand-alone wind tunnel that has been modified for boundary-layer transition studies. The objective of establishing a Blasius boundary layer with a high degree of spanwise uniformity has been frustrated by the persistence of Klebanoff modes, i.e., weak streamwise vortices within the layer. The vortices originate at the leading edge and appear to be caused by almost immeasurably small nonuniformities in the freestream introduced by the wind-tunnel screens. The vortices cause a spanwise thickening and thinning of the layer. Contours of the background unsteadiness in a spanwise plane through the layer show locally concentrated regions with elevated levels that are associated with the vortices. These contours are used as a sensitive indicator for the flow quality improvements. Although far from forming a complete parametric study, the observations should act as a valuable guide for others. For example, spanwise variations in the porosity of the screens were discovered by traversing each screen between a laser and a photo detector. Significant improvement in the spanwise uniformity of the layer was obtained by sorting the screens based on these results. The quantities that are generally agreed upon to define acceptable flow quality proved to be inadequate during the final stages of refinement. The background unsteadiness within the layer has been reduced by a factor of 30 compared with the initial configuration.

Nomenclature

h_e	= height of exit slot (see Fig. 1), mm
h_i	= height of leading edge (see Fig. 1), mm
M	= screen mesh (number of wires per lineal inch)
P	= pressure, Pa
R	= Reynolds number (dimensionless)
U	= streamwise velocity, ms^{-1}
U_1	= freestream velocity, ms^{-1}
u	= rms of streamwise velocity fluctuations, ms^{-1}
(x, y, z)	= coordinate system; origin is the centerline of the leading edge, mm or m
δ	= 99% boundary-layer thickness, mm
δ_1	= displacement thickness, mm
η	= boundary-layer coordinate: $y(U_1/\nu x)^{1/2}$ (dimensionless)
λ	= spanwise wavelength, mm
ν	= kinematic viscosity, m^2s^{-1}

Subscripts

d	= diameter
max	= maximum quantity
ref	= reference quantity

Introduction

EXPERIMENTAL investigations of boundary-layer transition require an extremely low background disturbance level, i.e., vortical and acoustic disturbances in the freestream originating from tunnel components such as the fan. Controlled disturbances can then be deliberately introduced and their characteristics measured to validate advanced numerical techniques, such as the parabolized stability equation method, or to justify the use of simplifying analytical assumptions, e.g., linear stability theory. One especially troublesome source of background disturbances is associated with weak streamwise vortices, which can appear as concentrated regions of elevated background unsteadiness. The phenomenon was first noted by Klebanoff and Tidstrom,[1] who studied the evolution of two-dimensional Tollmien–Schlichting (TS) waves generated by a vibrating ribbon in a flat-plate boundary layer. They found an almost periodic spanwise variation of the mean flow with rms unsteadiness levels u/U_1 of up to 5% and a spanwise wavelength of $\lambda_z \approx 5\delta$. The source of the variations was eventually traced to the wind-tunnel screens. In a later experiment, with improved screens, Klebanoff et al.[2] still found spanwise variations of the same wavelength, but they were much smaller in magnitude. Klebanoff[3] investigated the effect of freestream turbulence and found that the spanwise variations are associated with unsteadiness at low frequencies that should be stable according to linear stability theory.[4] The phenomenon has been studied in some detail by Kendall,[5,6] who named the phenomena Klebanoff modes. He found that $\lambda_z \approx 2\delta$ in his experiment and that the amplitude of the unsteadiness grows as $x^{1/2}$ to reach values as large as 5% before the onset of instability.

Currently, it is not possible to provide a rigorous definition of a Klebanoff mode. However, the present consensus is that Klebanoff modes are associated with local regions of concentrated streamwise vorticity. There appears to be a distinction between the spatially fixed vortices that are connected with freestream nonuniformity (e.g., Ref. 7) and unsteady vortices associated with freestream turbulence (e.g., Ref. 8). The term Klebanoff mode is strictly a misnomer because the vortices locally distort the flow, and therefore (by definition) they are nonlinear phenomena; e.g., the growth rate of TS waves is altered.[9]

Detrimental nonlinear interactions can occur between the controlled disturbances of interest and the Klebanoff modes. These interactions remain poorly understood, yet they could be responsible for the differences that are often observed between the measured and calculated TS wave behavior, for example. The work described in this paper demonstrates the immense care required to obtain the high flow quality required for meaningful transition investigations. In particular, a tremendous effort has been required to reduce the magnitude of the remarkably persistent Klebanoff modes to an acceptably small level.

Original Configuration of the Facility

The facility is a small-scale, stand-alone wind tunnel that was previously used for turbulent boundary-layer investigations[10] The flow was provided by a centrifugal blower driven by a variable speed dc motor. Three turbulence generating grids were used to enhance the mixing in the diffuser downstream of the fan. An aluminum honeycomb with hexagonal cells was installed after the diffuser

Presented as Paper 97-0228 at the AIAA 35th Aerospace Sciences Meeting, Reno, NV, Jan. 6–9, 1997; received Feb. 3, 1997, revision received Oct. 1, 1997; accepted for publication Oct. 26, 1997.

*Senior Research Scientist, Mail Stop 260-1, NASA Ames Research Center. Senior Member AIAA.

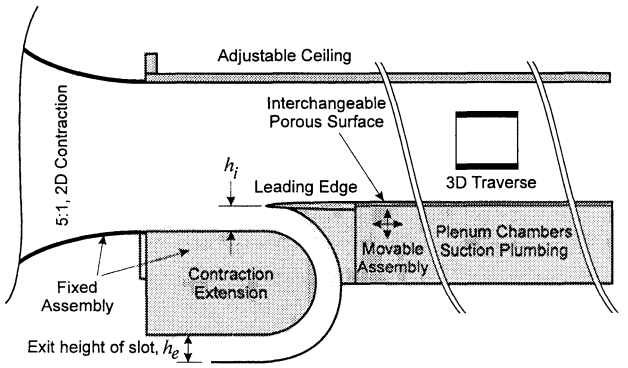

Fig. 1 Schematic of 1-m-wide test section showing plenum chambers and associated suction plumbing for porous surface studies and nomenclature for setting stagnation point.

followed by four stainless-steel turbulence damping screens. A new two-dimensional contraction and a 1-m-wide test section were added when the author started work on a direct numerical simulation validation study concerning turbulent boundary layers in pressure gradients. The freestream unsteadiness within the test section was 0.12%, and the spanwise distribution of turbulent skin friction on the test surface was within ±2%. In this original form, the facility was representative of small-scale research wind tunnels found within universities, and the flow quality was adequate for significant work concerning turbulent flows, e.g., Ref. 11.

Substantial modifications to the facility were made by Watmuff[12] for studies concerned with disturbances generated by suction holes used for laminar flow control. A two-dimensional elliptic leading edge of 24:1 aspect ratio was built to establish a new laminar boundary layer on an interchangeable porous surface that is supported by a baffled plenum chamber box. It is common practice to support laminar flow test surfaces on legs within the test section and to set the stagnation point by adjusting a hinged flap attached to the rear of the test surface. The depth of the plenum chamber box and associated plumbing below the interchangeable porous surface prohibited this type of installation, and so the following alternative was developed. Curved sheet metal is attached to the underneath of the leading edge. The sheet metal acts in conjunction with an extension to the contraction exit to form a curved slot for redirecting the excess test section flow, i.e., below the leading edge, out into the laboratory. The location of the leading edge can be adjusted with respect to the exit of the contraction. The leading-edge stagnation point is set by adjusting the exit height of the slot that controls the rate of excess airflow into the laboratory. The relationship between these components can be seen in Fig. 1. Wool tuft visualization indicates that the flow in the slot is steady and everywhere attached. The method has been found to perform as anticipated. For example, reducing the exit height of the slot causes the flow to attach to the underneath of the leading edge. For an extreme setting, a separation bubble forms on the upper surface leading to a turbulent boundary layer on the test surface shortly after the reattachment.

Preliminary Measurements and Techniques

A high-speed computer-controlled three-dimensional probe positioning system is integrated into the test section. A microVAX 3600 computer is used to control tunnel speed, probe traversal, and data acquisition. Standard Dantec boundary-layer single hot-wire probes were modified for all mean flow and unsteadiness measurements. The standard 1-mm-long, 5-μm-diam wires were replaced with 0.5-mm-long, 2.5-μm-diam tungsten wires. The wires are operated using a custom-built anemometer.[13] A high-speed 15-bit analog-to-digital converter is used for double-buffered data acquisition and processing. High-speed algorithms are used for processing the hot-wire data in real time.[14] A considerable investment in both hardware and software has enabled all experimental procedures to be totally automated. Operation of the facility has been refined to the point where experiments can be performed continuously (24 h per day) over several weeks without scheduled manual supervision.

In the original configuration, the onset of intermittent bursting on an impervious surface was observed at a Reynolds number $R_x \approx 2.25 \times 10^6$, which was believed to be acceptable for the porous surface investigations. Preliminary measurements were made by Watmuff[15] using isolated suction holes on the impervious test surface used to establish the base flow. Harmonic disturbances were applied to the isolated holes using a small loudspeaker for two cases, i.e., with and without net suction applied to the hole. Phase-averaged data were measured on spatially dense three-dimensional grids to examine the evolution of the three-dimensional TS waves for each case. The case without net suction applied to the hole approximates the idealized harmonic point source (HPS). Although the behavior of two-dimensional disturbances is relatively well understood, it is remarkable that substantial differences exist between the results of various computational methods and between experiments for this case of the simplest possible form of three-dimensional disturbance in the simplest possible flow. Consequently, the measurements attracted the attention of several computationalists and data were exchanged for comparison purposes.[16]

Figure 2a shows the mean velocity and Fig. 2b the rms unsteadiness profiles obtained at $\Delta x = 0.1$ m intervals along the centerline of the test section for a unit Reynolds number of 1.25×10^6 m^{-1}. The hot-wire signals were not filtered before sampling, but all quantities were obtained as the average of 10 sets of consecutive ensemble averages, consisting of 5000 samples each and acquired at 5 kHz, i.e., a total sampling period of 10-s duration. Note that this procedure introduces a digital form of ac coupling. The experimental uncertainty in U is estimated to be ±1%, and for u the uncertainty is estimated to be ±2%. The mean velocity profiles in Fig. 2a conform to the Blasius profile. However, the rms unsteadiness levels in Fig. 2b are moderately large and the location of the peak values

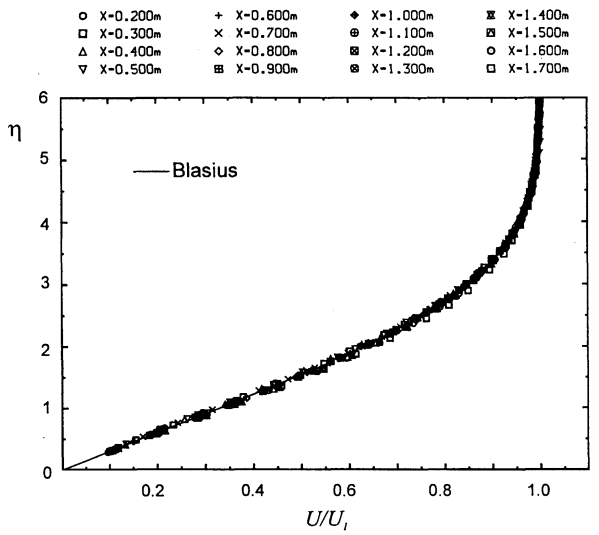

a) Streamwise velocity U/U_1

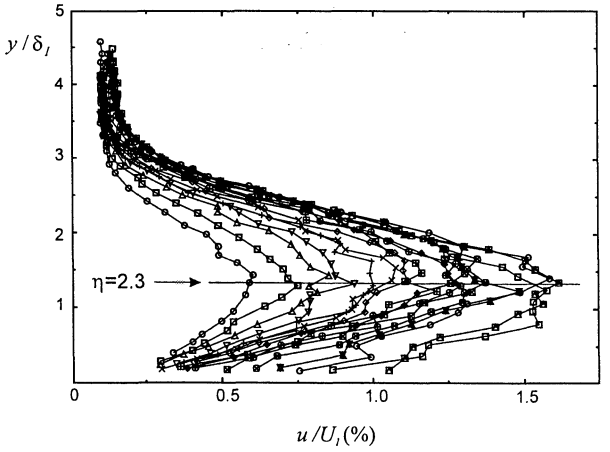

b) RMS background unsteadiness u/U_1

Fig. 2 Hot-wire profiles at $\Delta x = 0.1$ m intervals along centerline of test section. Original configuration.

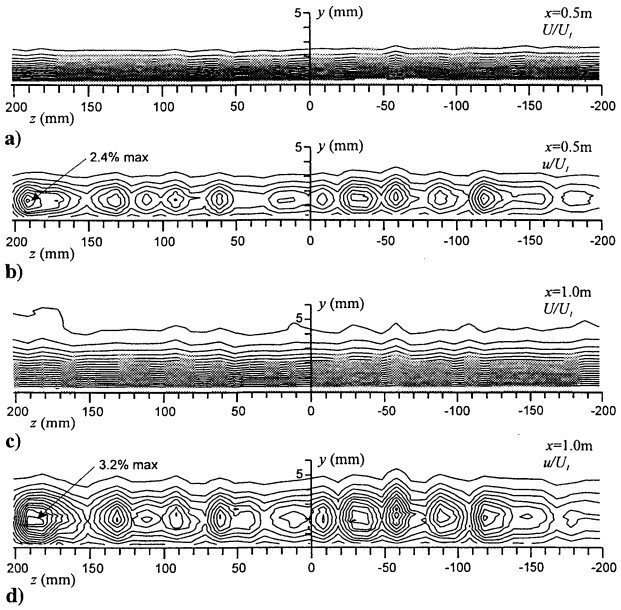

Fig. 3 Contours of streamwise velocity U/U_1 and rms background unsteadiness u/U_1 in two spanwise planes for original configuration. Contour increment for U/U_1 = 0.05 and for u/U_1 = 0.25%. Grid details: (Ny, Nz) = (29, 41), 1189 data points, and spacing Δz = 10 mm.

is $\eta \approx 2.3$, which is larger than what would be expected from TS waves. The location of the peak amplitudes is consistent with the Klebanoff modes observed by Kendall.[5,6] Figures 3a–3d show the corresponding mean flow and unsteadiness contours obtained on two spanwise planes, i.e., $x = 0.5$ and 1.0 m. Locally concentrated regions of elevated rms background unsteadiness are clearly evident together with spanwise variations in the layer thickness. These measurements illustrate the pitfall of the common practice of only measuring profiles on the centerline to demonstrate concordance with the two-dimensional Blasius boundary layer.

Corresponding contours of the rms three-dimensional TS wave amplitude generated by the HPS (Ref. 12) show considerable distortion when viewed in a spanwise plane. The distortion is associated with the Klebanoff modes, and it makes comparison with corresponding calculations by Mack and Herbert[16] almost meaningless. It became evident that the Klebanoff modes would need to be removed, or at least significantly reduced in amplitude, before the layer would be ready for meaningful fundamental studies. Therefore the HPS (without suction) was chosen as the logical starting point for validation of 1) the overall flow quality of the experimental facility and 2) various computational methods.

Known Effects of Wind-Tunnel Screens

Wind-tunnel screens are normally installed in the settling region upstream of the contraction to reduce 1) nonuniformity of the mean flow uniformity and 2) turbulence intensity. Much of the theoretical and experimental information on the turbulence damping characteristics of screens can be found in the reviews by Corrsin[17] and Laws and Livesey.[18] The theoretical treatment of turbulence suppression by screens ignores the additional turbulence generated by the screen and cannot consider details of the physical phenomena in the immediate vicinity of the screen. Instead, the screen is usually characterized by the open area ratio and a loss coefficient, and the reduction of turbulence is expressed in terms of these parameters. Although the predicted reduction factors are in qualitative agreement with observations, there is considerable scatter in the experimental data.

Screens may be further characterized by the Reynolds number based on the wire diameter, i.e., R_d. Vortex shedding by the wires will occur for $R_d \geq 40$. In this situation the screens are referred to as supercritical. Tan-atichat et al.[19] studied the effects of screens and perforated plates on freestream turbulence for a variety of incoming flow conditions. They suggested that the mesh size for supercritical screens should be chosen so that the length scales of the turbulence generated by the screen are smaller than those of the incoming turbulence. Groth and Johansson[20] investigated the effect of a range of screen parameters on carefully documented freestream turbulence generated by a rectangular grid of square rods. For a given open area ratio they found that the turbulence damping characteristics of a screen increase for decreasing mesh size. They observed that the anisotropy downstream of a screen is larger than for a turbulence grid, with up to 90% of the turbulent energy contained in the lateral velocity fluctuations. The anisotropy also has a smaller rate of decay with streamwise distance compared with grid turbulence. They found that a combination of a coarse and a fine screen gave at least as effective turbulence suppression as a pair of fine screens.

A less widely appreciated effect of screens is the additional benefit of suppressing boundary-layer separation. This is an important consideration in wind-tunnel diffusers. For example, Mehta[21] found that the effect of a screen was to reduce the layer thickness, which made it less susceptible to separation. The same benefit would be expected with the turbulence grids used in this facility. More recently, Seltsam[22] used a Reynolds-averaged numerical method to calculate the effect of various screen combinations on diffuser performance. The predicted improvements were implemented in a wind tunnel and led to experimentally verified flow improvements. Seltsam's numerical results are noteworthy because they demonstrate the experimentally observed lens effect of screens, and both the upstream and downstream influence of a screen on the mean flow are in qualitative agreement with the limited number of observations.

New Screens and Original Centrifugal Fan

Inspection of the four original wind-tunnel screens revealed that the tension was quite low and nonuniform. The screens had been stapled and glued to wood frames, which appeared to have undergone subsequent distortion. The original screens were replaced with eight new high-quality screens. Special emphasis was placed on achieving a high and uniform tension of the screen cloth. The stress exerted on a frame by a highly tensioned screen can be large and so stiff screen frames were constructed using a solid aluminum extrusion of section 75 × 25 mm. As noted earlier, Groth and Johansson[20] recommend using a cascade of screens with decreasing mesh size in the streamwise direction. They recommend using supercritical screens because of the smaller pressure drop characteristics leading to reduced power requirements. However, power consumption was not a significant factor for this small-scale facility. Furthermore, they observed improved turbulence damping characteristics with a smaller mesh size for a given open area ratio. Therefore a strategy was adopted of using the finest mesh, with the largest open area together with an overall constraint of using the highest quality cloth available. The screen cloth was selected by visually inspecting several batches with a magnifying glass. The screens were manufactured in pairs utilizing the stainless steel cloths specified in Table 1.

Various techniques were explored for stretching the stainless steel screen cloth with a high degree of uniformity while bonding with epoxy onto the solid aluminum frame. The stretching of stainless steel cloth with a high degree of tension and uniformity is deceptively difficult. It became clear during early testing that any method that holds the screen cloth locally to the frame is unsatisfactory. An example of an unsatisfactory technique is the common practice of stapling the cloth to wood frames. This technique should be avoided, even if the wood frames are to be used only as temporary stretching frames. A description of the three screen fabrication methods is given in Ref. 23. The best screens were produced by a subsidiary of the screen cloth supplier, who offers a screen installation service to the food and mining industries. They use a technique where the screen cloth is sandwiched between reusable rubber-faced

Table 1 Screen cloth specification for first set of eight screens (four pairs of each type of cloth)

Screen cloth	Mesh, in.$^{-1}$	Wire diam., in.	Open area, %	R_d
1	28	0.0075	62.4	47.6
2	44	0.0055	57.5	34.9
3	46	0.0045	62.9	28.6
4	56	0.0040	60.2	25.4

bars that are controlled pneumatically. A device that measures the screen tension in different directions is used to ensure an extremely even tension while epoxy is used to bond the screen cloth to the frame. A total of six screens (three pairs) were constructed using the finest meshes listed in Table 1. Two coarse $28M$ screens were also installed at the exit of the diffuser, upstream of the honeycomb. All of the screens are seamless.

Flow quality is generally quantified by the rms unsteadiness of the freestream. This quantity showed a significant improvement with the eight new screens, i.e., $u/U_1 = 0.08\%$ compared with $u/U_1 = 0.12\%$ with the old screens. However, a much greater improvement was observed in the layer; i.e., the peak rms background unsteadiness was reduced by a factor of 3.

Mean velocity and rms background unsteadiness measurements were made in a spanwise plane at $x = 1.0$ m ($R_x = 1.25 \times 10^6$) for a number of settings of h_e and h_i (see Fig. 1 for definitions). The optimum configuration was taken to be that with the most uniform spanwise distribution, which was determined by trial and error. Several interesting features are worth noting in these measurements as shown in the background unsteadiness contours in Figs. 4a–4d. The contours correspond with two settings of h_i and a range of h_e. When the height of the leading edge is increased from $h_i = 38.1$ (Fig. 4a) to 42.9 mm (Fig. 4b), a new peak level emerges. The magnitude of this new peak decreases with increasing h_e, as shown by the dashed line labeled 1 in Figs. 4c and 4d. Increasing h_e causes the stagnation point to move to the upper surface of the leading edge. The peak level observed along the dashed line labeled 2, for $h_i = 38.1$ mm in Fig. 4a, almost completely disappears when $h_i = 42.9$ mm, as shown in Fig. 4b. The dependency of the contours on h_e and h_i was found to occur in all test configurations.

Also note that the maximum levels in Figs. 4a–4d are located closer to the wall compared with the original configuration shown in Figs. 3b and 3d. This observation is consistent with the notion of increased TS wave activity for the combination of the new screens with the old centrifugal blower. Following the measurements in the spanwise plane, a set of centerline mean velocity and broadband unsteadiness profiles was initiated at $\Delta x = 50$ mm intervals, and intermittent bursting was found to occur at $x = 1.2$ m, i.e., $R_x = 1.50 \times 10^6$. This is a very interesting observation because intermittent bursting with the old screens was found to occur at $x = 1.8$ m ($R_x = 2.25 \times 10^6$); i.e., the Reynolds number for the onset of bursting with the new screens was 67% of that observed with the old screens. An explanation for this seemingly anomalous behavior is provided later.

The original centrifugal blower had nine curved sheet metal blades that contribute to quieter operation than straight blades. The design is characterized by an impeller that is relatively small compared with the casing. This feature allows the blower to operate over a wide range of speeds and pressures. However, wool tuft visualization studies revealed that flow separation occurs within the casing. Furthermore, viewing the wool tufts with a stroboscopic light source revealed that the separation is highly unsteady and appears to be correlated with the angular position of the blades with respect to the blower outlet. The power spectral density of the hot-wire signals in the test section indicated that a large proportion of the freestream unsteadiness occurs within a narrow band surrounding the blade-passing frequency. Spectral measurements within the layer also showed the presence of disturbances at this frequency. It is likely that the acoustic disturbances in the freestream originating from the passage of the fan blades introduce TS waves into the layer by some receptivity mechanism in the vicinity of the leading edge.

The seemingly anomalous behavior mentioned earlier, i.e., improved flow quality but transition at lower R_x, can be explained by noting that larger-amplitude Klebanoff modes were present in the layer with the old screens. Interactions between Klebanoff modes and TS waves are a subject of current study. There is some evidence to suggest that Klebanoff modes suppress the growth of TS waves. If this is generally true, then the reduced magnitude of the Klebanoff modes observed with the new screens would allow the blade-passing-induced TS waves to grow more rapidly and thereby cause the bursting to occur at a lower Reynolds number.

Considerable time was spent adjusting the pressure/flow-rate requirements of the tunnel in an attempt to reduce the magnitude and the frequency of the disturbances introduced by the blower. However, none of these tests was successful, and the centrifugal blower was replaced with a high-flow quality axial fan.

New Screens and New Axial Fan

The new axial fan has adjustable blade angles, and the installation required substantial modifications to the tunnel. To minimize low-frequency unsteadiness due to separation, an internal diffuser cone was fabricated and attached to the rear of the fan casing to form a nacelle that protruded into the diffuser. A 90-mm-thick cellular rubber section was also added between the fan and the diffuser, and it substantially reduces the vibration transferred from the fan to the tunnel. Turbulence grids are a major source of pressure loss, but the vigorous mixing generated by the turbulence behind the grids reduces large-scale unsteadiness and helps to achieve a uniform flow in the diffuser. Additional $1.33M$ turbulence grids were added to the tunnel, e.g., between the flanges of the fan and rubber vibration isolator.

Installation of the new fan reduced the rms unsteadiness of the freestream, i.e., $u/U_1 = 0.05\%$, and spectral measurements indicate that approximately half of the energy occurs at a frequency below 10 Hz. Figure 5 shows the rms background unsteadiness in a spanwise plane within the layer at $x = 1.0$ m for the unit Reynolds number of 1.25×10^6 m^{-1}. Comparison with Figs. 4a–4d shows that the peak levels of the background unsteadiness have been further reduced by a factor of 3.5 after installation of the new fan. Note that the peak levels are now located farther from the wall, i.e., at a position similar to

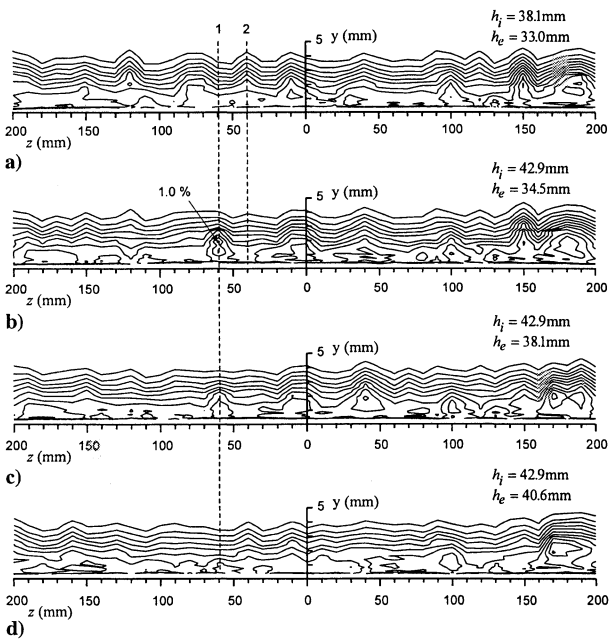

Fig. 4 Contours of rms background unsteadiness u/U_1 in spanwise plane at x = 1.0 m with new screens and original centrifugal blower for range of leading-edge heights h_i and slot exit heights h_e as labeled. Contour increment = 0.10%. Grid details: (Ny, Nz) = (29, 41), 1189 data points, and spacing Δz = 10 mm.

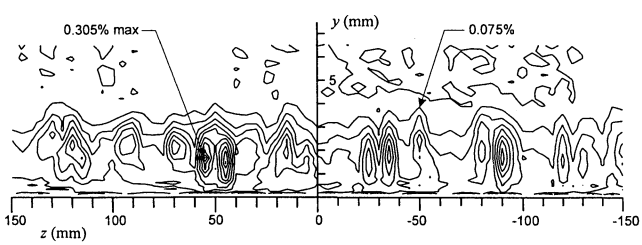

Fig. 5 Background unsteadiness u/U_1 in spanwise plane at x = 1.0 m, with axial fan and new screens sorted on basis of visual judgment of screen quality. Contour increment = 0.025%. Grid details: (Ny, Nz) = (31, 61) = 1891 data points, and spacing Δz = 5 mm.

the background disturbances observed in the original configuration as shown in Fig. 3d. This is further evidence that the background unsteadiness observed with the new screens and the old centrifugal blower combination (Figs. 4a–4d) have a significant TS component. Despite an order of magnitude reduction in the background disturbance level, the Klebanoff modes were still found to persist within the layer, and further refinements were required.

Laser Scanning of Wind-Tunnel Screens

Kendall has experienced similar difficulties in removing Klebanoff modes from the boundary layer in his tunnel. He was unable to detect any nonuniformity in the freestream upstream of the leading edge. However, he used a laser to scan his screens and found variations in the uniformity of the weave of the cloth. He observed a substantial improvement in the spanwise uniformity of the mean flow and a reduction in the rms background unsteadiness within the layer by changing the order of the screens based on these measurements; i.e., he ordered the screens from least to most uniform in the flow direction.

Following Kendall's observations, all of the subcritical screens were scanned with a laser using the method shown schematically in Fig. 6a. Two edges of the screen ride on linear bearings, and the screen is traversed between a fixed laser and photo detector. The motion of the screen causes rotation of a multiple turn potentiometer whose output voltage is calibrated against a linear scale. The resolution of the digitized potentiometer signal corresponds to less than 0.025 mm of movement. The diameter of the laser beam was not measured with precision, but it is estimated to be about 2.5 mm, which corresponds to about four or five mesh lengths for the subcritical screens. Portion of a high resolution (0.05-mm sample interval) laser scan of a $46M$ screen is shown in Fig. 6b. The influence of individual mesh wires moving into and out of the beam are evident, and they cause a fluctuation of about 2.5% of the mean photo detector output.

The laser scans were performed along lines corresponding to the position of the leading edge after flow through the contraction. The screens are rectangular, and so it is possible to install them with two possible orientations. Laser scans were performed using both orientations for each of the six new subcritical screens. Of particular concern was the most downstream $44M$ screen, which had a variation of 7.5% of the mean photo detector output. The results for both ends of this screen are shown in Fig. 7 for the full range of traversal.

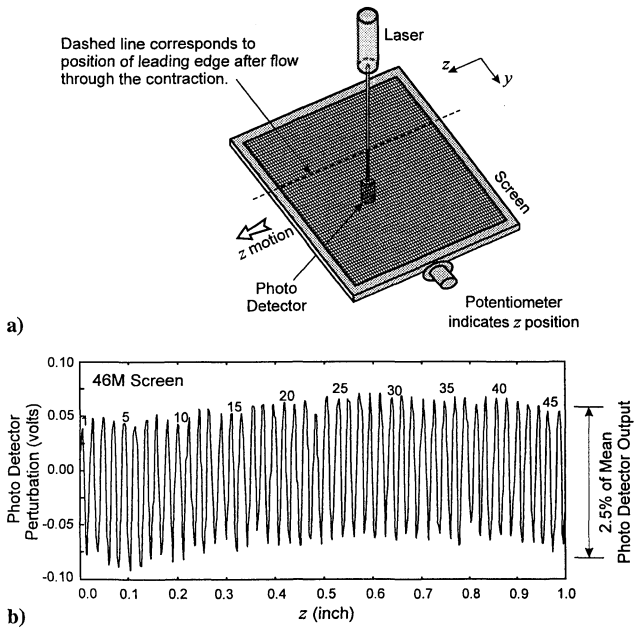

Fig. 6 a) Schematic showing technique for laser scanning of wind-tunnel screens to determine spanwise variations in the porosity. b) Portion of a high-resolution (interval $\Delta z = 0.05$ mm) laser scan of $46M$ screen. Individual wires can be resolved as labeled and cause approximately 2.5% variation in the photo detector output.

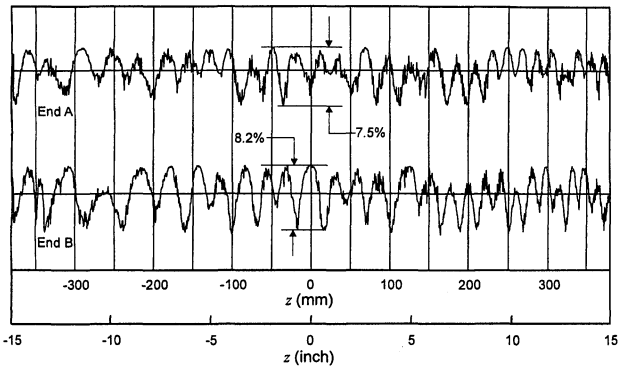

Fig. 7 Open area variation (perturbation of photo detector output) of both usable ends of most downstream screen as determined by laser scan. This screen was judged best by visual inspection but found to be the worst after laser scans.

Variations as large as this cannot be attributed to the effect of individual wires, i.e., 2.5%, as shown in Fig. 6b. These larger variations are most likely associated with imperfections in the weave of the screen cloth, which are presumably introduced during the manufacturing process. Another disturbing feature in the results is that the imperfections are not aligned at each end. For example, the end labeled A in Fig. 7 has an open area maximum in the vicinity of $z \approx -100$ mm, whereas this position corresponds to an open area minimum for the end labeled B. The different characteristics observed at each end of the same screen cannot be attributed to misalignment between the screen cloth and the frame because the alignment was within one or two mesh lengths over the entire length of the frame. The difference in the open area variations is of some concern because it implies that a single laser scan may not be sufficient to characterize a screen.

Most authors, e.g., Tan-atichat et al.,[19] recommend that screens be ordered from the coarsest to the finest mesh in the flow direction. However, because the screens are subcritical, i.e., $R_d < 40$, the screen order was not believed to be as important as the screen quality. This particular $44M$ screen had been selected for the most downstream location based on the subjective judgment of screen quality, which was determined by visual inspection. Furthermore, visual inspection of the finest $56M$ screens revealed that they appeared to be the most nonuniform, and they were installed in the most upstream location. However, laser scans of the $56M$ screens revealed instead that they were the most uniform.

Screen Order Based on Laser Scans

The order of the screens in the flow direction was changed to follow the results of the laser scans, i.e., from least to most uniform. The corresponding contours of the background unsteadiness in a spanwise plane at $x = 1.0$ m, i.e., $R_x = 1.25 \times 10^6$, are shown in Fig. 8b. Comparison with Fig. 5 shows that the effect of reordering the screens has reduced the peak background unsteadiness by a factor of 1.5. The contours in Fig. 8b are also more evenly distributed than those in Fig. 5 and do not have the conspicuous localized concentrations of elevated background unsteadiness. Despite these improvements, it is evident that the Klebanoff modes persist within the layer, and the corresponding distortion of the three-dimensional TS wave amplitude contours was still found to exist.

Freestream Uniformity Measurements

As mentioned earlier, Kendall was unable to detect a spanwise variation in the freestream velocity upstream of the leading edge. In his case, it can only be conjectured that the improvement in spanwise uniformity of the layer was due to a corresponding improvement in the uniformity of the freestream. Direct observation of the exceedingly small spanwise nonuniformities in the freestream could reveal a direct connection with the appearance of the Klebanoff modes in the boundary layer as well as provide a direction for further controlled studies. A number of attempts were made to measure the small variations in freestream velocity using a highly accurate

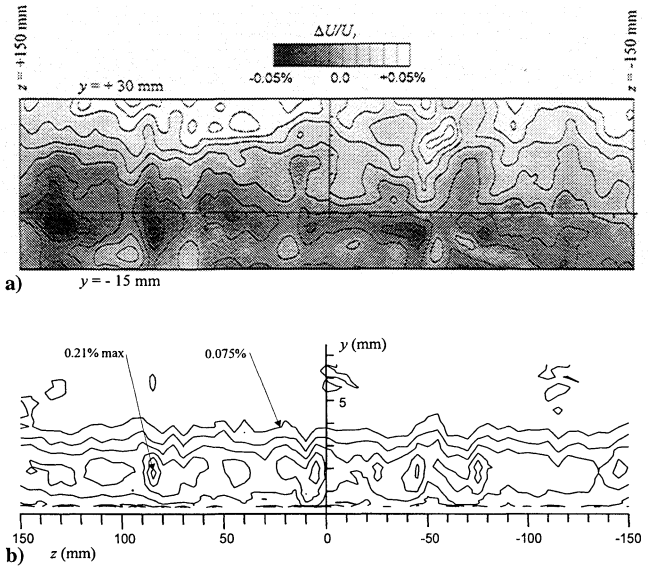

Fig. 8 a) Almost immeasurably small freestream velocity variation contours on plane 63 mm upstream of leading edge. Grid details: (Ny, Nz) = (46, 301), 13,846 data points, and spacing Δz = Δy = 1 mm. b) Corresponding background unsteadiness u/U_1 within layer. Same as per Fig. 5 but with screens ordered according to results of laser scan.

differential pressure transducer that is maintained at constant temperature by an internal electric heater element. The transducer has a full scale of 125 Pa (0.5 in. of water), and from observation over several years it has proved to have exceedingly small drift with ambient temperature and time. The method that produced the most consistent and repeatable results used a traversing total pressure tube connected directly to the transducer and a fixed total pressure tube connected directly to the reference pressure port. Data were measured on a 1 × 1 mm resolution grid with $(Ny, Nz) = (46, 301)$ data points using circular total pressure tubes of 1-mm external diameter. A total sampling time of 30 s was used for each of the 13,846 data points requiring a total run time of around five days of continuous operation.

It should be emphasized that the differences in total pressure are exceedingly small; i.e., the difference between the maximum and minimum pressures over the entire grid corresponds to 0.42 Pa (0.0017 in. of water). By repeating the measurements at a single point on more than 100 occasions during a 24-h period, the uncertainty in the total pressure difference (ΔP) at a given point was estimated to be within ±0.025 Pa (±0.0001 in. of water). The grid measurements were obtained as profiles of varying y at a constant z. The repeatability of the measurements was further checked by measuring a subset of the grid as profiles of varying z at a constant y. The contours of ΔP in the region of overlap were essentially the same and independent of the different order for the traversal of the planar grid.

Contours of the corresponding variation in freestream velocity ($\Delta U/U_1$) are shown in Fig. 8a. The contours have been calculated assuming that the total pressure variations (ΔP) are entirely attributable to differences in dynamic pressure, i.e.,

$$\Delta U/U_1 \approx -\tfrac{1}{2}\Delta P/P_{\text{ref}}$$

where P_{ref} is the reference dynamic pressure of 210 Pa (0.84 in. of water). The coordinate axes shown in Fig. 8a are referenced to the test surface and the leading edge is located along the line $y = -6.35$ mm in this coordinate system.

The most pertinent features in the contours are the spanwise variations because it is likely that they are somehow related to the Klebanoff modes that appear in the layer. Note the overall reduced level corresponding to deceleration approaching the leading edge. When the upstream influence of the leading edge is taken into account, the spanwise variations have an elongated streakiness in the y direction. A direct comparison of the freestream variations in Fig. 8a and the corresponding Klebanoff modes in the layer shown in Fig. 8b reveals a consistent relationship in areas where the freestream variations are pronounced. Regions of reduced freestream velocity, e.g., $90 < z < 100$ mm, and $-50 < z < -40$ mm, are associated with regions of elevated background unsteadiness levels and increased layer thickness (not shown). The nonuniformity of the most downstream screen (end A in Fig. 7) does not reveal a direct correlation with the flow variations. Evidently the upstream screens still exert some influence on the flow.

Effect of Leading-Edge Geometry

The appearance of regularly spaced spanwise disturbances in the nominally two-dimensional flow past the leading edge of blunt-nosed bodies has been known since the 1930s (see Ref. 24 for a comprehensive review). A long-standing controversy has existed over whether the source of the vortices is a local instability mechanism or an inherent feature of the two-dimensional viscous stagnation line flow. A recent theoretical analysis by Dhanak and Stuart[25] concerning the stagnation flow of a two-dimensional cylinder tends to support the latter hypothesis. Their work suggests that the dominant parameter is the ratio of the cylinder diameter to the spanwise length scale of the freestream nonuniformities. Of particular interest is their result indicating that the streamwise vorticity does not appear for wavelengths of the freestream nonuniformity below a critical value. Assuming their results to be applicable to the elliptic leading edge, then changing the radius of curvature of the tip might be expected to have an influence on the strength of the Klebanoff modes in the boundary layer.

The elliptic leading edge was modified by adding a wedge-shaped extension with a 3-deg half-angle. The modified leading edge is 75 mm longer and the radius of curvature is an order of magnitude smaller than the elliptic leading edge. Examination of the mean flow and rms background unsteadiness contours measured in a spanwise plane at $x = 1.0$ m ($R_x = 1.25 \times 10^6$) indicated that the appearance and spacing of the Klebanoff modes were much the same and independent of the modifications to the radius of curvature.

Inviscid computations (using a two-dimensional panel method) for both the modified sharp leading edge and the elliptic leading edge reveal that the pressure distribution in the vicinity of the junction with the flat plate is much the same for these two configurations. The pressure distribution in this region is characterized by a small adverse pressure gradient owing to the discontinuity of the second derivative of the surface contour. A new leading edge was built with an upper surface based on a superelliptic profile shape, i.e.,

$$(x/a)^m + (y/b)^2 = 1$$

with $a = 203$ mm, $b = 3.8$ mm, and $m = 4$. The radius of curvature of the tip is larger than the elliptic profile shape. The inviscid calculations for this profile shape revealed a smooth monotonic pressure variation in the vicinity of the junction with the flat plate. Nevertheless, the results for this new leading edge were also disappointing because the appearance and spacing of the Klebanoff modes were much the same as for the sharp leading-edge configuration.

These disappointing results do not necessarily mean that the analysis of Dhanak and Stuart[25] is inapplicable to a different geometry. For example, one possibility is that the freestream nonuniformities contain a multitude of spanwise scales and that a different leading-edge radius of curvature selectively amplifies a different range of scales. However, assuming a correspondence between the cylinder diameter and the leading-edge radius of curvature, it should also be noted that the spanwise length scales predicted from their analysis are considerably smaller than those observed in the boundary layer. Therefore another possibility is that some form of merging of fine-scale streamwise vortices occurs and that the merging is determined by the viscous length scales of the downstream boundary layer.

Final Configuration

Additional high-quality screens (using solid aluminum frames) were installed while the sharp leading edge, i.e., with wedge-shaped tip, was employed. However, the comparison with the superelliptic leading edge was performed using the same screen configuration. Three of the new high-quality screens are located upstream of the honeycombs and are of relatively coarse mesh, i.e., $12M$, $24M$, and $24M$. Nine screens are located downstream of the honeycombs.

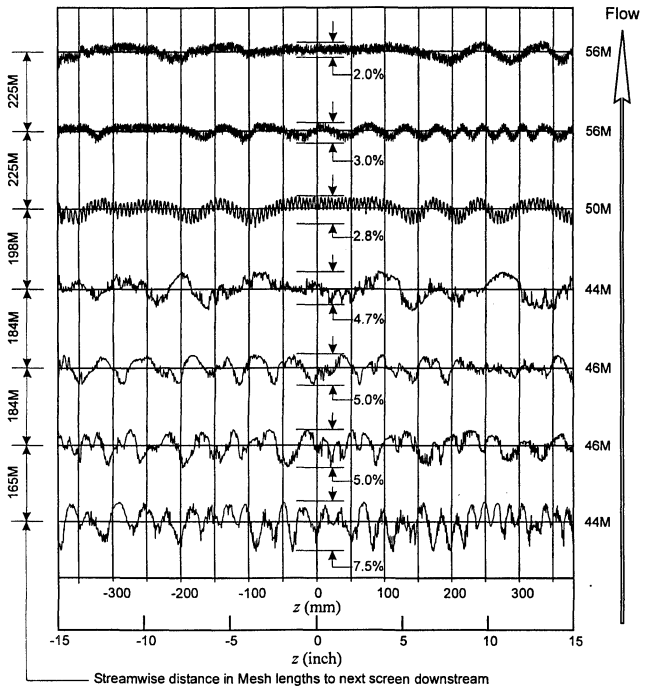

Fig. 9 Open area variation determined by laser scans of the most uniform ends of the seven most downstream (subcritical) screens for the final configuration. Screen mesh and open area (photo detector) variation are labeled.

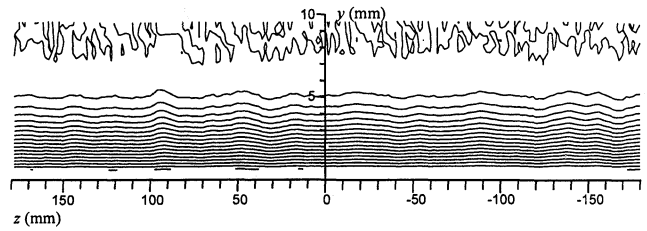

a) Streamwise velocity U/U_1 with contour increment = 0.05

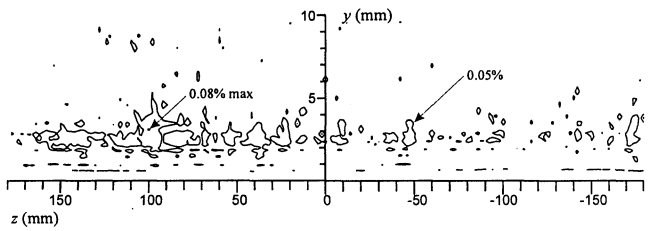

b) Background unsteadiness u/U_1 with contour increment = 0.025%

Fig. 10 Hot-wire measurements in a spanwise plane at x = 1.0 m for final configuration. The background unsteadiness has been reduced by a factor of 30 compared with the original configuration at a comparable Reynolds number (see Fig. 3b). Grid details: (Ny, Nz) = (31, 180) = 5580 data points and spacing Δz = 2 mm.

The first two screens are also relatively coarse mesh, i.e., each $22M$, whereas the remaining seven screens are subcritical. All of the subcritical screens were laser scanned for uniformity, and the results are shown in Fig. 9, which is the same screen order as the final configuration. However, the tests with the sharp and superelliptic leading edges were performed with a streamwise spacing between the screens that is less than that shown in Fig. 9.

Several other modifications were made to the facility as outlined next. The screen spacing was increased to around 200 mesh lengths in the streamwise direction as shown in Fig. 9. The length of the settling region between the last screen and the contraction was doubled. The entrance to the test section was lengthened by 380 mm, placing the leading edge farther downstream of the contraction exit. The combined effect of all these modifications did have some beneficial effect, leading to a reduction of the rms background unsteadiness in the boundary layer by a factor of approximately 1.5.

Most experimental data and numerical results are available for the HPS using the Mack–Kendall parameters.[16] The unit Reynolds number was reduced from 1.25×10^6 to 0.668×10^6 m^{-1} to accommodate these parameters. An added benefit is that all screens downstream of the honeycomb are subcritical at this lower unit Reynolds number. Contours of the rms HPS generated three-dimensional TS waves measured in a spanwise plane were considerably improved and showed only minimal distortion by the Klebanoff modes, at least close to the leading edge. However, the effect of the Klebanoff modes became observable, and their influence eventually became significant on the three-dimensional TS amplitude contours, with increasing streamwise distance from the source.

The last modification to the tunnel was inspired by informal discussions with M. Tobak of NASA Ames Research Center. Tobak has observed the presence of streamwise vorticity over a period of many years in a variety of low-speed and high-speed flows. He has recently developed some new topological ideas concerning the effect of pressure gradient on separation and attachment. Our discussions led to the hypothesis that the formation and growth of the Klebanoff modes might be sensitive to the local pressure gradient very close to the tip of the leading edge. A pressure undershoot is typically located just downstream of the stagnation point in the two-dimensional flow over a round nosed airfoil at zero angle of attack. The recovery, from this undershoot, to the zero pressure gradient on the flat plate leads to a region of adverse pressure gradient.

In an effort to control the local pressure gradient, a length of flexible ceiling was installed, extending from the contraction exit to about halfway along the leading edge. The ceiling was contoured to impose an external favorable pressure gradient (FPG) in the vicinity of the leading edge. Adjustment of ceiling contour was performed by trial and error, using measurements in the boundary layer as feedback. The measurements consisted of spanwise profiles of the rms background unsteadiness at a fixed height of $y = 2.1$ mm, at the streamwise position $x = 1.5$ m downstream of the leading edge, using the lower unit Reynolds number of 0.668×10^6 m^{-1}, i.e., $R_x = 1.0 \times 10^6$. This streamwise position was selected because it corresponds to where corner flow disturbances have propagated out to a point corresponding to the extremity of the three-dimensional TS waves generated by the HPS located upstream at $x = 0.412$ m. The benefit of the FPG is substantial, and at some spanwise positions, it is responsible for reducing the background disturbance level by more than a factor of 2.

The mean flow and rms background unsteadiness contours obtained in a spanwise plane located at $x = 1.0$ m ($R_x = 0.668 \times 10^6$) are shown for the final configuration in Figs. 10a and 10b. Comparison of Fig. 10b with Fig. 3b reveals that the rms background disturbance level within the layer has been reduced by a factor of 30 for a comparable Reynolds number. However, there are still some small spanwise variations in the thickness of the layer. Analysis of the 180 mean velocity profiles used to produce Fig. 10a reveal a ±6% variation in displacement thickness over this span, whereas the corresponding variation in shape factor is within ±2%. Measurements of the HPS generated three-dimensional TS waves for the final configuration are presented by Watmuff,[26] and the rms wave amplitude distribution is now in substantial agreement with the corresponding calculations presented by Mack and Herbert.[16]

Conclusions

The evidence is almost overwhelming that the Klebanoff modes in the boundary layer are caused by nonuniformities in the freestream that originate from variations in the weave of the wind-tunnel screen cloth. The appearance of Klebanoff modes in the boundary layer show a remarkable sensitivity to these almost immeasurably small freestream nonuniformities. Parametric studies are needed to account for the observations presented in this paper and other unresolved issues concerning wind-tunnel screens. For example, at the most fundamental level, it is not completely understood why supercritical screens generate fine-scale turbulence with widely different properties to grid turbulence. A refinement of the screen model and Reynolds-averaged calculation method could establish a relationship between freestream nonuniformities and the open area

variations of screens. Of a more practical concern is that subjective visual examination of the screen cloth can be deceptive. Laser scanning of the screen cloth provides a quantitative measure of the porosity variations. However, laser scans of the same screen cloth indicate that the variations in the porosity can be dissimilar at different locations.

Measurements that are generally accepted as quantifying flow quality, e.g., rms unsteadiness of the freestream, proved to be inadequate and insensitive indicators of the improvements. Further work is required to establish more stringent specifications for acceptable flow quality. These specifications will be particularly relevant for testing models with laminar flow control devices in large-scale production wind tunnels. Such a study might explain why tests performed with the same model in different wind tunnels often produce such widely differing results. The extraordinary sensitivity of the formation of streamwise vortices in the boundary layer suggests that a special body (or family of bodies) be developed for the specific purpose of quantifying wind-tunnel flow quality.

Acknowledgments

All experiments were performed in the Fluid Mechanics Laboratory Branch at NASA Ames Research Center. Additional funding was provided by the Director's Discretionary Fund. Many helpful discussions with A. J. Dietz are acknowledged. Consultations with M. Tobak concerning the influence of local pressure gradients on the origin of the vortices proved extremely valuable. The author especially wishes to thank J. M. Kendall of the Jet Propulsion Laboratory for examination of results as they came to hand and for willingly offering advice throughout the course of this work. He provided useful and unpublished information concerning the difficulties he has experienced attempting to rid the boundary layer of Klebanoff modes in his wind tunnel, and he also provided unpublished data concerning the properties of the Klebanoff modes. His encouragement to persist with the effort after the many disappointing results is most appreciated.

References

[1]Klebanoff, P. S., and Tidstrom, K. D., "Evolution of Amplified Waves Leading to Transition in a Boundary Layer with Zero Pressure Gradient," NASA TN D-195, Sept. 1959.

[2]Klebanoff, P. S., Tidstrom, K. D., and Sargent, L. M., "The Three-Dimensional Nature of Boundary-Layer Instability," *Journal of Fluid Mechanics*, Vol. 12, 1962, pp. 1–34.

[3]Klebanoff, P. S., "Effect of Free-Stream Turbulence on a Laminar Boundary Layer," *Bulletin of the American Physical Society*, Vol. 16, No. 11, 1971, p. 1323.

[4]Herbert, T., and Lin, N., "Studies of Boundary-Layer Receptivity with Parabolized Stability Equations," AIAA Paper 93-3053, July 1993.

[5]Kendall, J. M., "Experimental Study of Disturbances Produced in a Pre-Transitional Laminar Boundary Layer by Weak Freestream Turbulence," AIAA Paper 85-1695, June 1985.

[6]Kendall, J. M., "Boundary Layer Receptivity to Freestream Turbulence," AIAA Paper 90-1504, June 1990.

[7]Goldstein, M. E., Leib, S. J., and Cowley, S. J., "Distortion of a Flat-Plate Boundary Layer by Free-Stream Vorticity Normal to the Plate," *Journal of Fluid Mechanics*, Vol. 237, 1992, pp. 232–260.

[8]Westin, K. J. A., Boiko, A. V., Klingmann, B. G. B., Kozlov, V. V., and Alfredson, P. H., "Experiments in a Boundary Layer Subjected to Free Stream Turbulence. Part 1. Boundary Layer Structure and Receptivity," *Journal of Fluid Mechanics*, Vol. 281, 1994, pp. 193–218.

[9]Boiko, A. V., Westin, K. J. A., Klingmann, B. G. B., Kozlov, V. V., and Alfredson, P. H., "Experiments in a Boundary Layer Subjected to Free Stream Turbulence. Part 2. The Role of TS-Waves in the Transition Process," *Journal of Fluid Mechanics*, Vol. 281, 1994, pp. 219–245.

[10]Wood, D. H., and Westphal, R. V., "Measurements of the Free-Stream Fluctuations Above a Turbulent Boundary Layer," *Physics of Fluids*, Vol. 31, June 1988, pp. 2834–2840.

[11]Spalart, P. R., and Watmuff, J. H., "An Experimental and Numerical Study of a Turbulent Boundary Layer with Pressure Gradients," *Journal of Fluid Mechanics*, Vol. 249, 1993, pp. 337–371.

[12]Watmuff, J. H., "Boundary Layer Transition Studies," MCAT Inst., Final Rept. NCC2-698-95-12, NASA Ames Research Center, Feb. 1995.

[13]Watmuff, J. H., "A New High Performance Constant Temperature Hot-Wire Anemometer," NASA CR-177645, Aug. 1994.

[14]Watmuff, J. H., "High-Speed Real-Time Processing of Cross-Wire Data," *Experimental Thermal and Fluid Science Journal*, Vol. 10, 1995, pp. 75–85.

[15]Watmuff, J. H., "Interaction Between Instabilities Originating from Suction Holes," *Bulletin of the American Physical Society*, Vol. 38, Nov. 1993, p. 2237.

[16]Mack, L. M., and Herbert, T., "Linear Wave Motion from Concentrated Harmonic Sources in Blasius Flow," AIAA Paper 95-0774, Jan. 1995.

[17]Corrsin, S., *Turbulence: Experimental Methods. Handbuch der Physik*, Vol. 8, Pt. 2, Springer, 1963, pp. 524–590.

[18]Laws, E. M., and Livesey, J. L., "Flow Through Screens," *Annual Review of Fluid Mechanics*, Vol. 10, 1978, pp. 247–266.

[19]Tan-atichat, J., Hagib, H. M., and Loehrke, R. I., "Interaction of Free-Stream Turbulence with Screens and Grids: A Balance of Turbulence Scales," *Journal of Fluid Mechanics*, Vol. 114, 1982, pp. 501–528.

[20]Groth, J., and Johansson, A. V., "Turbulence Reduction by Screens," *Journal of Fluid Mechanics*, Vol. 197, 1988, pp. 139–155.

[21]Mehta, R. D., "Turbulent Flow Through Screens," AIAA Paper 84-0538, Jan. 1984.

[22]Seltsam, M. M., "Experimental and Theoretical Study of Wide-Angle Diffuser Flow with Screens," *AIAA Journal*, Vol. 33, No. 11, 1995, pp. 2092–2100.

[23]Watmuff, J. H., "Wind Tunnel Flow Quality Improvements," MCAT Inst., Progress Rept., Contract NAS2-14109, NASA Ames Research Center, Oct. 1995.

[24]Morkovin, M. V., "On the Question of Instabilities Upstream of Cylindrical Bodies," NASA CR-3231, Dec. 1979.

[25]Dhanak, M. R., and Stuart, J. T., "Distortion of the Stagnation-Point Flow Due to Cross-Stream Vorticity in the External Flow," *Philosophical Transactions of the Royal Society of London*, Vol. 352, 1996, pp. 443–452.

[26]Watmuff, J. H., "Interactions Between Klebanoff Modes and TS Waves in a Blasius Boundary Layer," AIAA Paper 97-0558, Jan. 1997.

R. W. Wlezien
Associate Editor